A New Cosmic Probe: Estimating High-Redshift Expansion from Nested Spiral Structures in Galaxy Rotation Curves

E.P.J. de Haas[1, a)]

Kandinsky College, Nijmegen, The Netherlands

We introduce a novel method for estimating the cosmic expansion rate H_z at high redshift using internal dynamics of nearby galaxies—without relying on redshift-distance observations. The approach models galaxy rotation curves that exhibit a clear transition between a central bar (interpreted as a relic spiral structure) and an outer spiral disk. Using a constant Lagrangian framework that separates metric inflow from virial motion, we identify galaxies requiring two distinct dynamical regimes. These nested structures are modeled with separate Lagrangians, enabling the extraction of H_z values from the inferred mass and critical radius of the proto-bar region—assumed to have formed with 5–20% of its present-day mass. Applying this method to seventeen galaxies yields independent H_z estimates corresponding to redshifts $z \sim 7$–29 and cosmic times between 100 and 700 Myr after the Big Bang. These values align with the expected epoch of early galaxy formation and provide an observationally grounded probe of cosmic expansion during the poorly constrained "Cosmic Dawn." This technique complements high-redshift observations (e.g., JWST, CMB extrapolations) and offers a new class of local dynamical constraints on the early universe. If validated and scaled, it could produce hundreds to thousands of independent H_z measurements, refining our understanding of baryonic structure formation and offering new insight into the timeline of cosmic expansion.

PACS numbers: 98.62.Dm, 98.80.-k, 98.80.Es, 98.62.Gq, 98.62.Ai

Keywords: Hubble parameter, galaxy rotation curves, early universe, nested spiral structure, cosmic expansion

[a)]Electronic mail: haas2u@gmail.com

I. OVERVIEW OF MODELING FRAMEWORK EVOLUTION

The theoretical framework presented in this paper evolved through a sequence of modeling refinements, each driven by the goal of improving the physical realism and explanatory power of galactic rotation curve fits. This progression not only deepens our understanding of galactic structure but ultimately enables a novel, physically grounded estimation of the local expansion rate H_z in the early universe.

We begin with a single-region model for individual galaxies, assuming a constant Lagrangian density within a symmetric baryonic bulge. In this regime, spiral inflow velocities can be expressed as a combination of tangential metric motion and radial metric components, encoded via a fixed effective potential. The effective potential incorporates Newtonian gravity and Hubble expansion through a superposition of respectivce metric velocities. This initial framework offers a good match for certain galaxies where the baryonic structure is dominated by a central bulge, but proves insufficient when confronted with more complex rotation curves.

To address this, the model is extended to incorporate *multi-region virial transitions*. By defining physically distinct domains—such as the bulge interior, a first pure spiral disk region, and an outer region with additional virial motion—the rotation curve can be decomposed into segments with different dynamical behaviors. This segmentation leads to more accurate fits and reveals structural transitions not visible in the single-region model.

However, some galaxies exhibit rotation curves that cannot be reproduced by a single global Lagrangian, even with multiple regions, but they allowed a fit usiing two constant Lagrangian curves. We now interpret these systems as displaying clear signatures of *nested spirals*: an inner, bar-like structure (interpreted as a relic spiral) and an outer disk spiral, each with distinct dynamical histories and possibly formed at different cosmic epochs. To capture this, the model is generalized to include two distinct Lagrangians—one for the inner bulge-bar spiral, one for the outer disk spiral—each characterized by its own radius, mass, and expansion parameter H_z. The outer disk spiral appears like a reset of the original bulge by including the mass of the bar and starts at the outer realm of the bulge-bar system, its visible or invisible ring with its specific critical radius.

Finally, by treating the inner bulge-bar as a fossil remnant of an earlier structural phase, ie a proto-galaxy, and assuming it constituted a small fraction (e.g., 5–20%) of today's bulge mass, we derive an independent estimate of the early-universe expansion rate H_z. This allows us to date the

emergence of these outer spiral structures, ie the onset of the disk's spiral, and compare the results to standard cosmological timelines. Strikingly, the inferred cosmic times align with the expected epoch of early galaxy formation, suggesting that this model may offer a novel and physically meaningful probe of high-redshift cosmic dynamics.

This hierarchical modeling—from single-region fits to nested spirals and cosmological interpretation—forms the backbone of the present analysis and underpins the results discussed in the sections that follow.

II. PROGRESSIVE ADAPTATION OF THE CONSTANT LAGRANGIAN INFLOW MODEL TO REAL GALACTIC DYNAMICS

A. Rotation Curve Fit for UGC 1281 Using the Metric Inflow Model

To assess the capability of the metric inflow model to describe real galactic rotation curves, we applied it to the dwarf galaxy UGC 1281. The primary objective was to determine whether the full radial profile of the orbital velocity squared $v^2(r)$ could be accurately reproduced using only parameters with direct physical interpretation—namely the bulge radius R, the enclosed mass M, and the cosmological expansion rate $H(z)$. The orbital velocity squared is modeled by two distinct regimes:

Inside the bulge ($r \leq R$):

$$v_{orb}^2(r) = \frac{1}{2}\left(\sqrt{\frac{2GM}{R}} - H_z R\right)^2 \cdot \frac{r^2}{R^2} \tag{1}$$

Outside the bulge ($r > R$):

$$v_{orb}^2(r) = \frac{3}{2}\left(\sqrt{\frac{2GM}{R}} - H_z R\right)^2 - \left(\sqrt{\frac{2GM}{r}} - H_z r\right)^2 \tag{2}$$

We began by manually estimating the bulge radius R_{bulge} using visual fitting techniques in a dedicated Excel analysis. This step aimed to identify the transition point between the inner solid-body rotation and the outer flattened region. Based on this inspection, we adopted $R_{\text{bulge}} = 1.968\,\text{kpc}$ as the best estimate and held it fixed during the automated fitting procedure. The best-fit parameters obtained were: Bulge mass: $M = 1.38 \times 10^{39}\,\text{kg}$; bulge radius $R = 1.968\,\text{kpc}$; Hubble parameter: $H_z = 2.30 \times 10^{-18}\,\text{s}^{-1}$; RMS relative residual: 0.065 (in units of km^2/s^2).

Figure 1 displays the best-fit v^2 curve, which shows excellent agreement with the full rotation curve of UGC 1281. The model accurately reproduces both the rising inner region and the extended flat portion without invoking a dark matter halo profile.

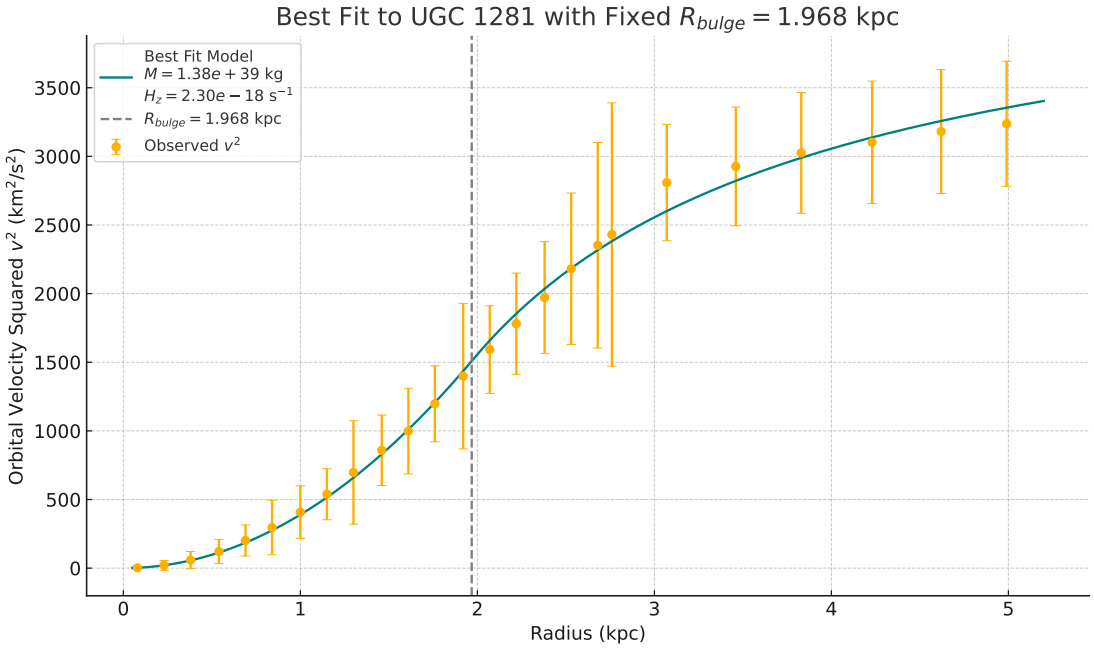

FIG. 1. Best-fit orbital velocity-squared profile $v^2(r)$ for UGC 1281, using the metric inflow model.

Figure 2 presents the residuals between the observed and modeled v^2, plotted with realistic error bars propagated from the velocity uncertainties. The distribution of residuals exhibits no systematic deviation and remains within observational noise levels, confirming the quality of the fit.

B. Interpretation of Outer Rotation Curve as Newtonian Orbit in a Moving Metric Frame

By examining the residuals and the behavior of the data in the outer disk, we identify the onset of a systematic deviation—visible as a consistent overshoot/undershoot in v^2_{data} compared to the model. More specifically, in Figure 2, the last six datapoints develop in a non random way from overshoot to undershoot. That is where we suspected a virial dynamics. By subtracting the inflow-predicted orbital velocity squared v^2_{model} from the SPARC rotation curve data, we isolated the residual component that, in our interpretation, corresponds to standard Newtonian motion.

As shown in Figures 3 and 4, the last six outermost datapoints of UGC 1281 yield residuals

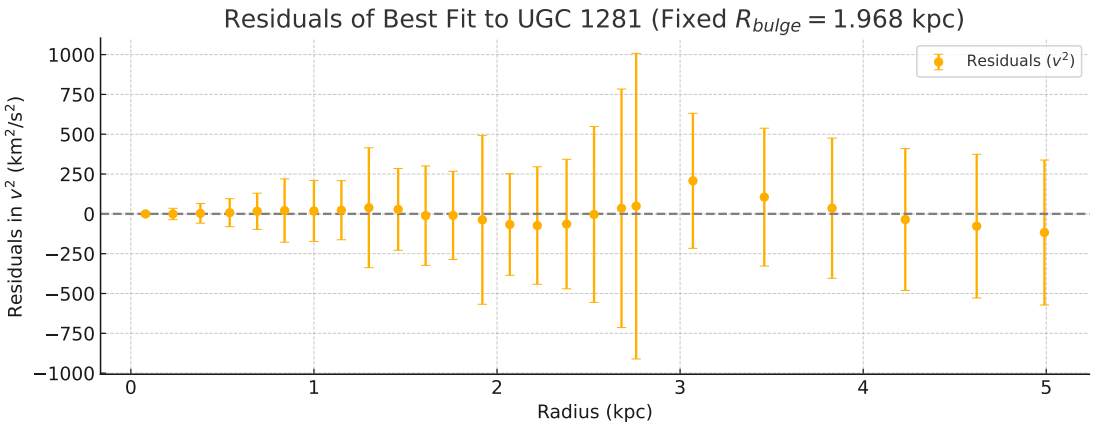

FIG. 2. Residuals in orbital velocity-squared v^2 between the observed rotation curve of UGC 1281 and the best-fit model using the metric inflow formalism. The bulge radius was fixed at $R_{\text{bulge}} = 1.968\,\text{kpc}$, while the mass M and the Hubble parameter H_z were fitted to minimize the weighted residual. Error bars reflect observational uncertainties propagated into v^2. The distribution is consistent with observational noise, supporting the quality of the fit.

that align closely with a Newtonian potential profile $v^2 = GM/r$, after applying a constant vertical shift. This shift accounts for the fact that the residuals are measured in the observer's frame, while the Newtonian orbit occurs within the local comoving metric frame of the orbiting material. The next question was how to incorporate this in the fitting model without tampering with the raw SPARC data.

We decided for continuation of the effective potential and thus introduced a virial term that for the involved masses acted as the only potential present, because relative to the inflowing metric to which they were inertially connected, they didn't experience any other force. The virial term is not applied uniformly but begins to contribute beyond a galaxy-specific radius r_{virial}, located somewhere between the bulge radius R and the critical inflow radius r_c. The value of r_{virial} is determined empirically through analysis of the residuals of the galaxy's rotation curve. In our three-region model, the transition between region 2 (bulge-dominated inflow dynamics) and region 3 (where additional virial orbital corrections are applied) is governed by a parameter r_{virial}. This radius is not directly derived from the analytic model but must be identified empirically. Specifically, we first fit the rotation curve using only regions 1 and 2. Once identified, we introduced a r_{virial} as a fixed input in the subsequent three-region fit. This two-stage approach ensures that the inclusion of the virial correction is not arbitrarily fitted but justified by a clear structural feature in

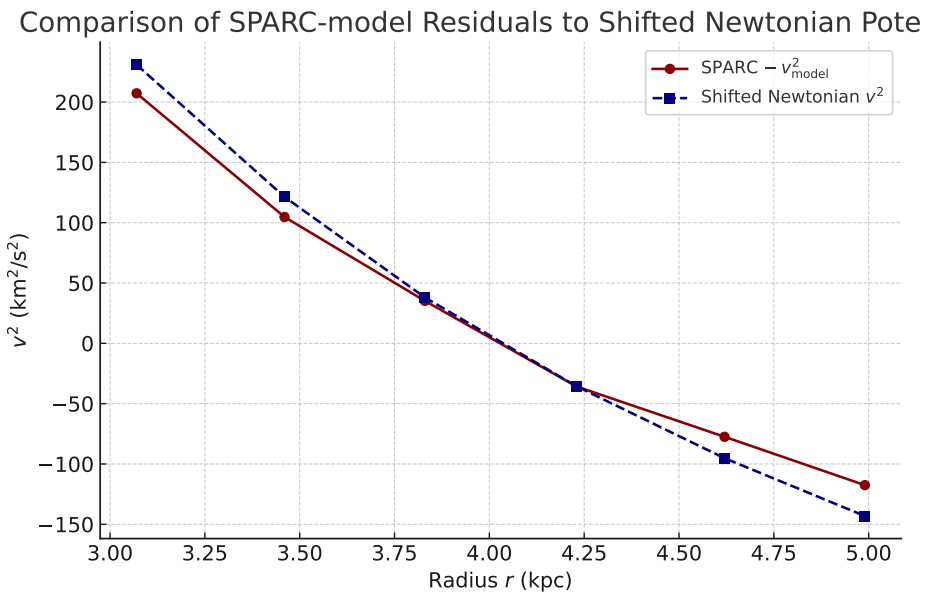

FIG. 3. Comparison of the SPARC–model residuals for the last six outermost data points of UGC 1281 (red circles) with a Newtonian orbital velocity squared profile (blue squares) based on the bulge mass $M = 1.38 \times 10^{39}\,\text{kg}$. The Newtonian curve $v^2 = \frac{GM}{r}$ was shifted vertically by $\Delta v^2 \approx -741.3\,\text{km}^2/\text{s}^2$ to match the residual profile. The agreement suggests that the outer residuals are consistent with a gravitational tail from the bulge alone, without invoking an additional dark matter halo or a modifacation of Newtonian dynamics.

the rotation curve. A parameter Φ_D is a gauge parameter for the virial term, which needs further explanation, but we will not examine that here.

C. Application to UGC 1281

In the case of UGC 1281, residuals from the original two-region metric model displayed a distinct systematic behavior in the outermost six datapoints. The observed v^2 first exceeded the predicted value and then dropped below it—characteristic of a transition to virial orbital motion.

Introducing the full virial term,

$$v^2_{\text{orb}}(r) = \frac{3}{2}\left(\sqrt{\frac{2GM}{R}} - H_z R\right)^2 - \left(\sqrt{\frac{2GM}{r}} - H_z r\right)^2 + \left[\frac{1}{2}\left(\sqrt{\frac{2GM}{r}} - H_z r\right)^2 - \Phi_D\right], \quad (3)$$

for $r \geq r_\Phi$, slightly reduced the RMS of the relative residual from approximately $6,5\%$ to $6,3\%$, demonstrating a small improvement in fit accuracy, see Figure 5 and Figure 6. This fit not only

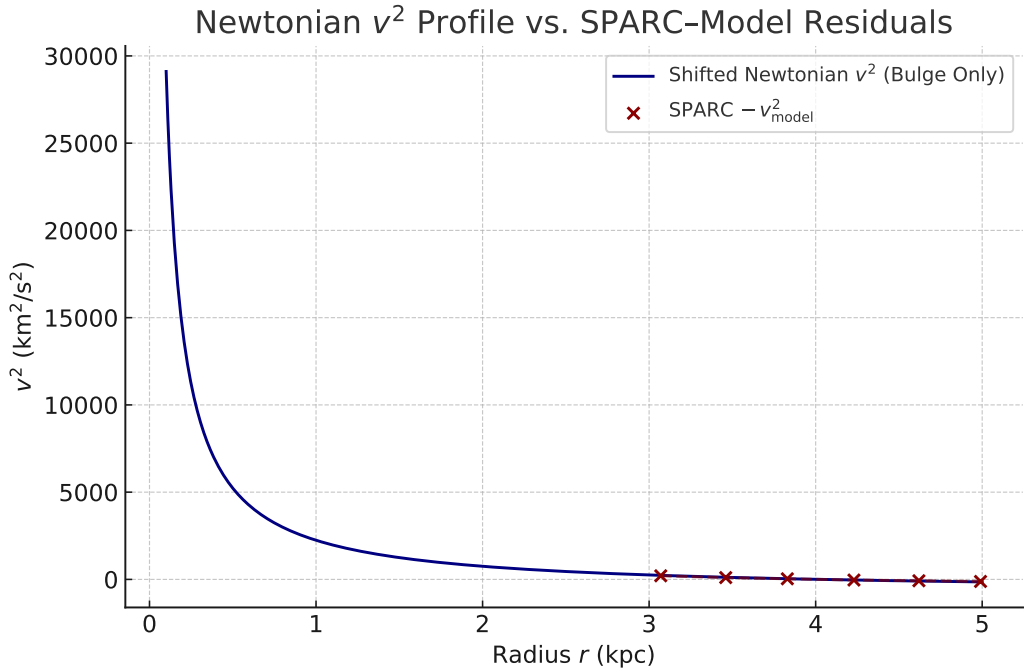

FIG. 4. Comparison between the Newtonian gravitational potential profile of the UGC 1281 bulge and the observed SPARC–model residuals. The blue curve shows the Newtonian orbital velocity squared, computed as $v^2 = \frac{GM}{r}$, for a bulge mass of $M = 1.38 \times 10^{39}\,\text{kg}$ and fixed radius. The curve has been vertically shifted by $\Delta v^2 \approx -741.3\,\text{km}^2/\text{s}^2$ to best align with the SPARC–model residuals from the outer six data points (shown in red). This alignment suggests that the residual structure is consistent with the Newtonian tail of the central bulge, reinforcing the model's interpretation that no additional halo is needed to explain the rotation curve.

reproduced the shape of the rotation curve but also corrected the systematic bias observed in the residuals, affirming the physical relevance of the virial contribution associated with disk dynamics.

D. The virial model applied to NGC 2366: two virial regions

A key success of the metric inflow model is its ability to iteratively improve the fit to galactic rotation curves through the structured inclusion of physically motivated corrections. We demonstrate this through a stepwise refinement of the velocity model applied to NGC 2366, for which we refined the virial term and introduced the possibility to introduce two virial terms for galactic rotation curves. This led to a potential four region approach:

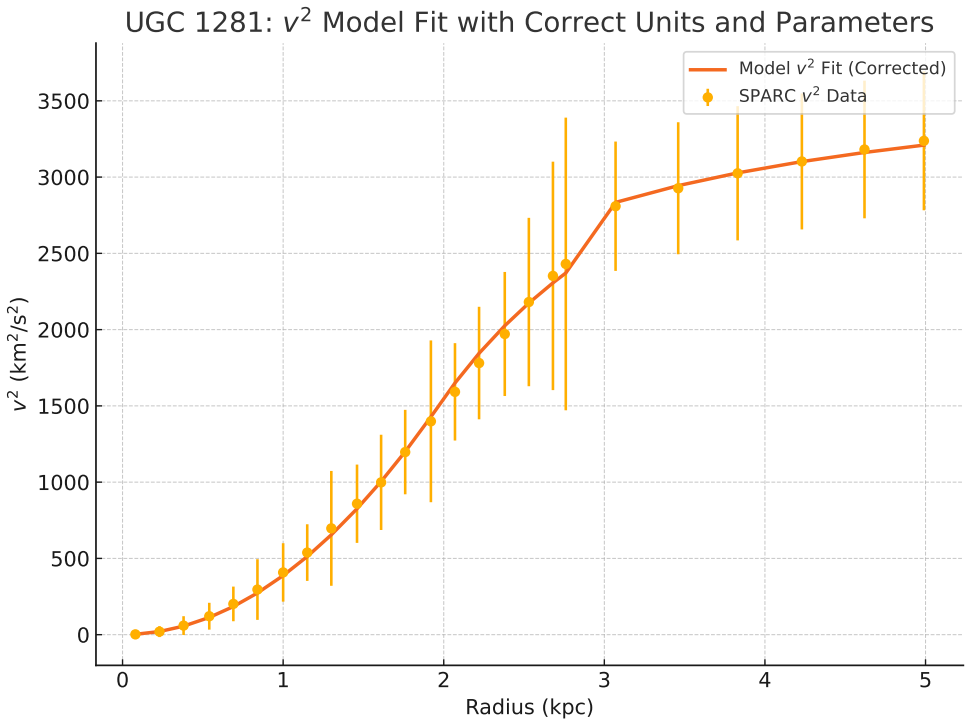

FIG. 5. Rotation curve fit for UGC 1281 using the three-region inflow metric model. The data points represent the observed SPARC rotation curve values v^2 with error bars. The model is constructed using three regions: (1) solid-body rotation inside the bulge, (2) Lagrangian inflow region from the bulge radius up to the virial transition radius, and (3) an outer region including a virial correction term. Model parameters: bulge radius $R = 1.97\,\text{kpc}$, virial transition radius $r_{\text{virial}} = 3.0\,\text{kpc}$, mass $M = 1.376 \times 10^{39}\,\text{kg}$, Hubble parameter $H_z = 2.1841 \times 10^{-18}\,\text{s}^{-1}$, and virial offset $\Phi_D = 716\,\text{km}^2/\text{s}^2$.

Inside the bulge ($r \leq R$)**:**

$$v_{orb}^2(r) = \frac{1}{2}\left(\sqrt{\frac{2GM}{R}} - H_z R\right)^2 \cdot \frac{r^2}{R^2} \tag{4}$$

Outside the bulge until the first virial region ($R < r < r_{virial_1}$):

$$v_{orb}^2(r) = \frac{3}{2}\left(\sqrt{\frac{2GM}{R}} - H_z R\right)^2 - \left(\sqrt{\frac{2GM}{r}} - H_z r\right)^2 \tag{5}$$

Outside the bulge for the first virial region ($r_{virial_1} < r < r_{virial_1}$):

$$v_{orb}^2(r) = \frac{3}{2}\left(\sqrt{\frac{2GM}{R}} - H_z R\right)^2 - \left(\sqrt{\frac{2GM}{r}} - H_z r\right)^2 + \left[p\frac{1}{2}\left(\sqrt{\frac{2GM}{r}} - H_z r\right)^2 - \Phi_p\right] \tag{6}$$

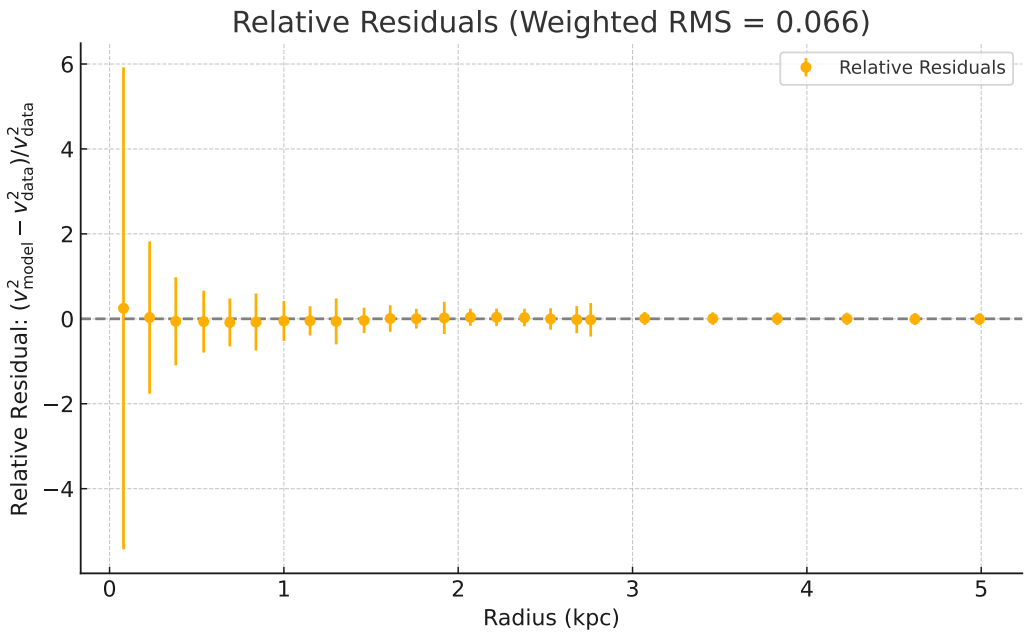

FIG. 6. Relative residuals of the rotation curve fit for UGC 1281 using the three-region Lagrangian inflow model with a virial correction beyond $r_{\text{virial}} = 3\,\text{kpc}$. The bulge radius was fixed at $R = 1.97\,\text{kpc}$, the bulge mass at $M = 1.376 \times 10^{39}\,\text{kg}$, the cosmic expansion rate at $H_z = 2.1841 \times 10^{-18}\,\text{s}^{-1}$, and the virial offset parameter $\Phi_D = 716\,(\text{km/s})^2$. The weighted root mean square (RMS) of the relative residuals is ~ 0.063, demonstrating excellent agreement between the model and the observational SPARC data.

Outside the bulge for the second virial region ($r_{virial_2} < r < rc$):

$$v^2_{orb}(r) = \frac{3}{2}\left(\sqrt{\frac{2GM}{R}} - H_z R\right)^2 - \left(\sqrt{\frac{2GM}{r}} - H_z r\right)^2 + \left[q\frac{1}{2}\left(\sqrt{\frac{2GM}{r}} - H_z r\right)^2 - \Phi_q\right] \quad (7)$$

We toke p and Φ_p and q and Φ_q as a free parametera, reflecting the natural history and orbital independence of the virial mass relative to the Lagrangian inflowing metric. The virial mass can flow with or against the Lagrangian tangential motion of the metric, its orbit can be in an inclined plane relative to the metric inflow of the spiral disk and it might be affected by the additional mass inbetween R and r_{virial}. So introducing two relatively free parameters per virial region seems theoretically and empirically justified. It allowed us to maintain the overal influence of M, R, and Hz over all regions. We define r_{virial} empirically, by visual inspection of the first virial free iteration of the fit of the rotation curve. After identification, the r_{virial} parameters setting the boundaries are fixed.

The result can be seen in Fig.(7), where we have two virial regions, with the first appearing

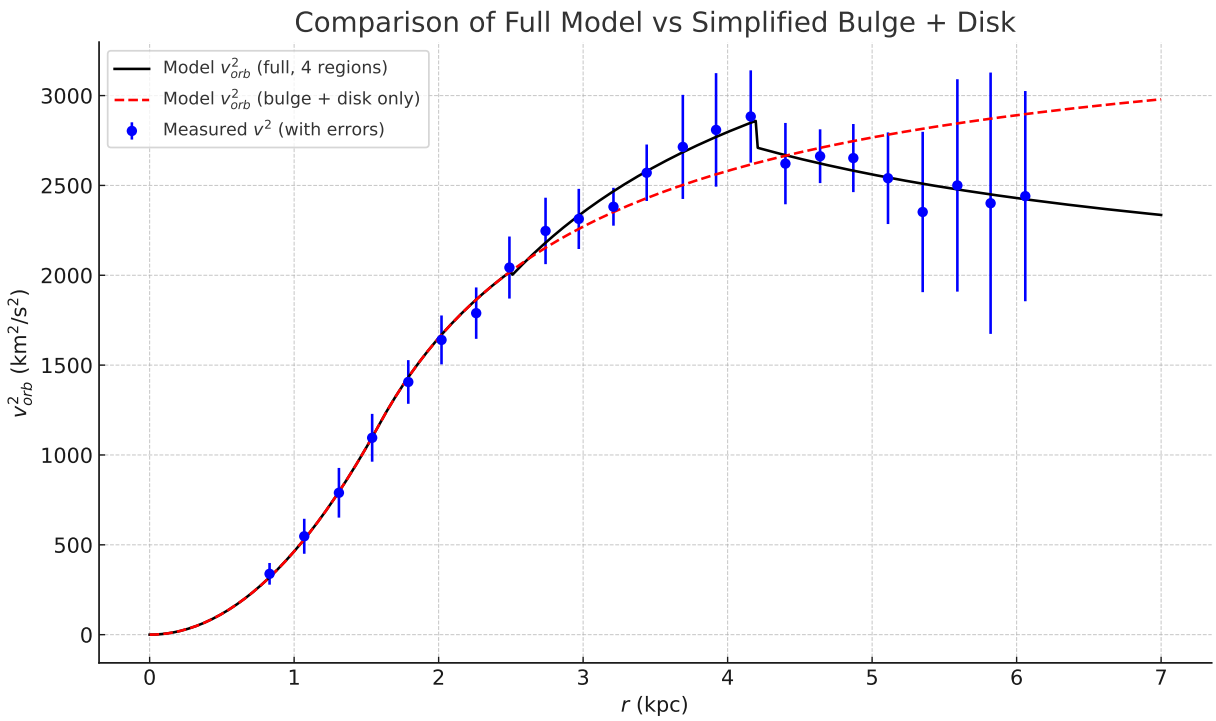

FIG. 7. Comparison between the full 4-region model (solid black) and the simplified bulge + disk model (dashed red) for the galaxy NGC 2366. The measured orbital velocities squared $v^2_{\rm orb}$ are shown as blue points with error bars. The simplified model does not account for virial effects and overpredicts v^2 at large radii.

as an overshoot relative to the Lagrangian orbital motion and the second one as on undershoot. The improved relative residuals can be seen in Fig.(8) and the RMS of the relative residuals was $2,73\%$.

E. Empirical justification for two parameters per virial region

Galactic mass distributions evolve through a non-uniform, episodic history of accretion, mergers, and localized gravitational collapses. This inherently stochastic process results in the presence of multiple dynamically distinct regions within a galaxy, some of which depart from the expected spiral inflow dictated by the background metric flow model. In our framework, the bulk of matter follows a Lagrangian metric inflow governed by three global parameters: the bulge mass M, the bulge radius R, and the Hubble-like expansion term H_z. This model predicts a smooth, continuous spiral velocity profile with a radial inflow component $v_{\rm eff}$ and an angular component $v_{\rm orb}$. The

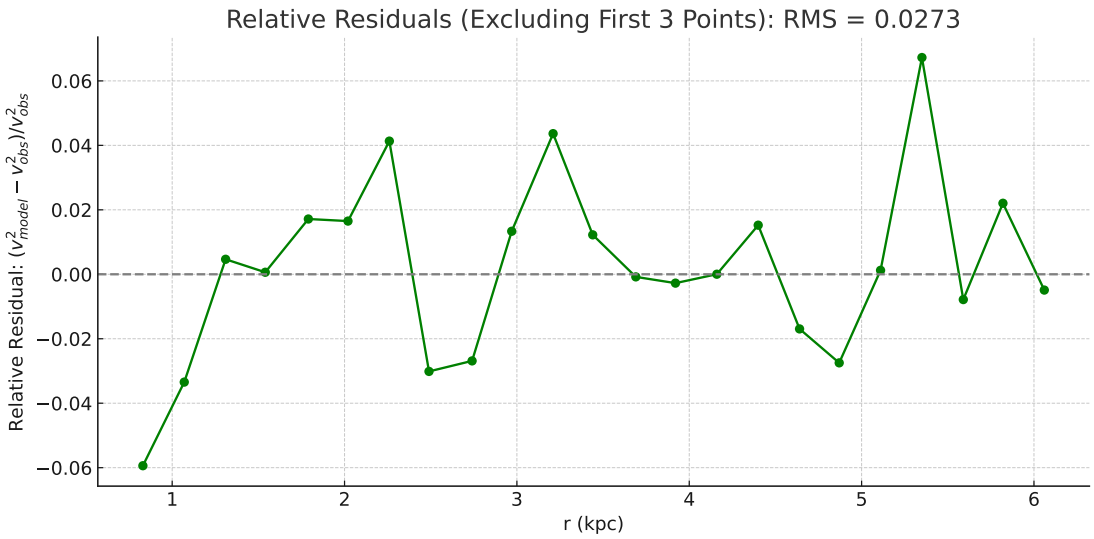

FIG. 8. Relative residuals of the squared orbital velocity model fit to the NGC 2366 rotation curve, excluding the first three data points. The RMS relative residual is approximately 0.0273, indicating a good fit in the outer regions.

resulting orbital velocity squared $v^2_{\rm orb}$ is illustrated in Fig.(7) (red dashed curve), which matches the observational data in the inner regions with high fidelity. However, deviations from this ideal spiral inflow occur in specific radial intervals, which we interpret as *virial zones*. These zones contain matter that has settled into local orbital configurations due to interactions or past accretion events, and thus no longer flows inward purely along the Lagrangian metric path. To capture these deviations, we introduce two additional parameters per virial region:

- A **virialization strength** parameter (p, q, ...), describing the degree to which the region deviates from the free-fall motion.
- A **potential offset** (Φ_p, Φ_q, ...), representing the effect of local disk mass distribution or substructures not included in the background bulge model.

Fig.(7) clearly demonstrates how the full model (solid black curve), which includes these virial corrections, improves agreement with the observed rotation curve. Notably, the outer regions of the galaxy show a significant departure from the red dashed spiral-inflow model, aligning instead with the modified curve that incorporates virialized motion.

This modeling approach thus offers a physically and dynamically justified structure: a coherent metric-based inflow with localized perturbations reflecting the galaxy's unique history. The

addition of two parameters per virial region provides the necessary flexibility to account for gravitationally bound orbital components without overfitting or abandoning the large-scale coherence of the model through the parameters M, R and Hz determining the dashed red curve and determining what counts as virial deviations.

III. FROM ONE SINGLE SPIRAL TO TWO SPIRALS: GALAXIES WITH A BULGE-BAR-RING-DISK NESTED SPIRAL MORPHOLOGY

In our original constant Lagrandian fit of the SPARC database galaxies, thirteen stood out because we needed two constant Lagrangians to fit the rotation curve. Each Lagrangian fit had its own radius and mass. It was as if the accumulation of mass forced a reset of the bulge. For the time, we didn't have an interpretation for this occurrence. Now we interpret it as nested spirals, ie bars, inside a larger spiral, ie the disk. So the previous three to four region fit, with bulge to disk to disk-with-virial-regions has to be enlarged with a bulge-bar to bar-as-new-bulge to disk to disk-with-virial-regions. The bulge-bar Lagrangian has its M, R set and so does the bar-as-new-bulge to disk to disk-with-virial-regions.

Inside the bulge ($r \leq R$):

$$v_{orb}^2(r) = \frac{1}{2}\left(\sqrt{\frac{2GM_{bu}}{R_{bu}}} - H_z R_{bu}\right)^2 \cdot \frac{r^2}{R_{bu}^2} \tag{8}$$

Outside the bulge, inside the bar until the onset of the disk ($R_{bulge} < r < R_{bar}$):

$$v_{orb}^2(r) = \frac{3}{2}\left(\sqrt{\frac{2GM_{bu}}{R_{bu}}} - H_z R_{bu}\right)^2 - \left(\sqrt{\frac{2GM_{bu}}{r}} - H_z r\right)^2 \tag{9}$$

Outside the bar, so on the disk, until the first virial region ($R_{bar} < r < r_{virial_1}$):

$$v_{orb}^2(r) = \frac{3}{2}\left(\sqrt{\frac{2GM_{bar}}{R_{bar}}} - H_z R_{bar}\right)^2 - \left(\sqrt{\frac{2GM_{bar}}{r}} - H_z r\right)^2 \tag{10}$$

Outside the bar for the first virial region ($r_{virial_1} < r < r_{virial_2}$):

$$v_{orb}^2(r) = \frac{3}{2}\left(\sqrt{\frac{2GM_{bar}}{R_{bar}}} - H_z R_{bar}\right)^2 - \left(\sqrt{\frac{2GM_{bar}}{r}} - H_z r\right)^2 + p\left[\frac{1}{2}\left(\sqrt{\frac{2GM_{bar}}{r}} - H_z r\right)^2 - \Phi_p\right] \tag{11}$$

Outside the bulge for the second virial region ($r_{virial_2} < r < rc$):

$$v_{orb}^2(r) = \frac{3}{2}\left(\sqrt{\frac{2GM_{bar}}{R_{bar}}} - H_z R_{bar}\right)^2 - \left(\sqrt{\frac{2GM_{bar}}{r}} - H_z r\right)^2 + q\left[\frac{1}{2}\left(\sqrt{\frac{2GM_{bar}}{r}} - H_z r\right)^2 - \Phi_q\right] \tag{12}$$

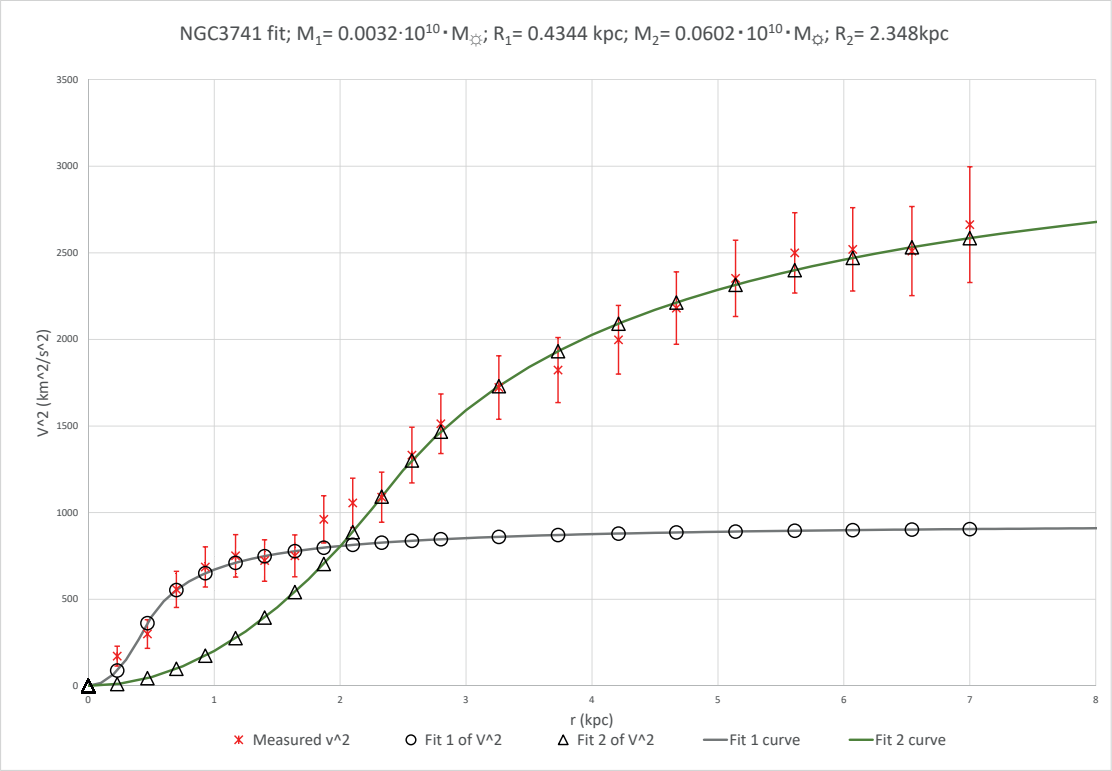

FIG. 9. Original, pre-Hz, two Lagrangian fit for galaxy NGC 3741. The RMS of the rel. residuals was 13%

In Fig.(9), the original, pre-Hz fit is given. In Fig.(10) one can see the result with two Lagrangians and one virial region with the effective potentials that include Hz expansion correction to the original Lagrangian. The values of the respective radii and masses are: $M_{bulge} = 7,36 * 10^{37} kg$, $R_{bulge} = 1,543 * 10^{19} m$, $M_{bar} = 1,09 * 10^{39} kg$, $R_{bar} = 7,129 * 10^{19} m$, and $Hz = 2.2 * 10^{-18} s^{-1}$. The relative residuals are given in Fig.(11) and the RMS of the relative residual was $6,8\%$. Around $r = 2kpc$, two data-points couldn't be fitted appropriately, with the interpretation that they marked the boundary between bar and disk and represent the transition from the one to the other.

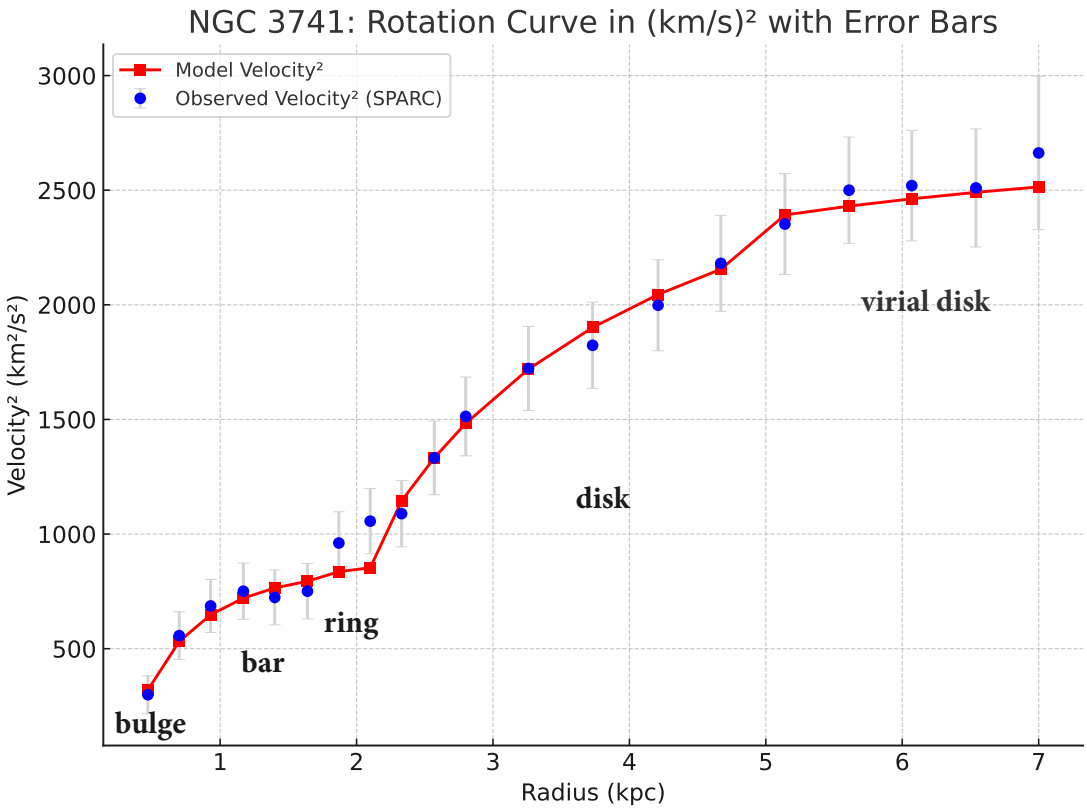

FIG. 10. Observed squared rotation velocities v^2_{obs} (blue circles) with error bars from SPARC data, compared to the model velocity squared v^2_{model} (red squares) for NGC 3741 as a function of galactocentric radius. $R_{bulge} = 0,537kpc$, $R_{bar} = 2,31kpc$ and $R_{virial} = 5,0kpc$, deviding the fit in four regions: bulge, bar, disk and virial disk.

IV. ESTIMATING THE FORMATION EPOCH OF THE PROTO-BAR FROM SIMPLE PHYSICAL INPUTS

In a previous paper we introduced the postulate that bars are nested spirals, beiing the proto-galaxy before its Lagrangian reset to a new 'bulge' to start evolving the spiral of the disk. We put forward the simple idea that the beginning of the spiral of the disk should be the critical radius of the bulge and the largest possible extend of the bar. This nested spiral, ending at its critical radius, thus ends as a ring, see Fig(12). This ring might or might not be a visible aspect of such a galaxies morphology. This should allow to find the Hz of the moment when the second spiral started to

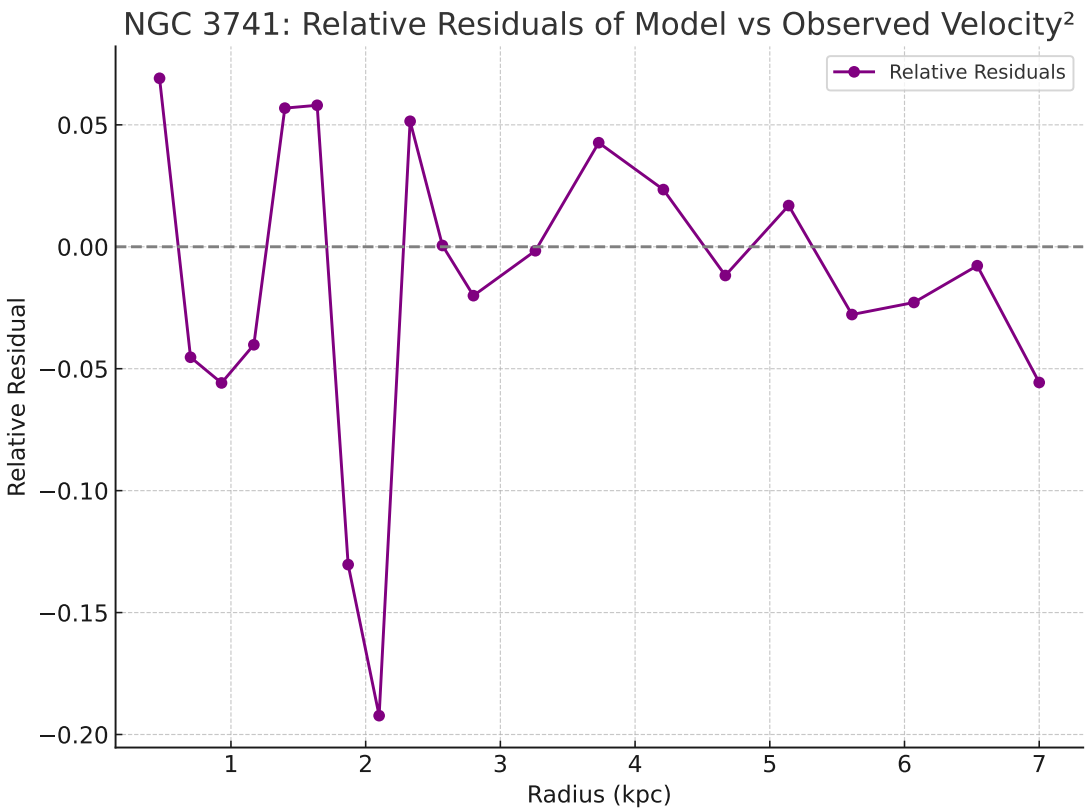

FIG. 11. Relative residuals $(v^2_{\rm model} - v^2_{\rm obs})/v^2_{\rm obs}$ for NGC 3741. The model closely matches the observed SPARC rotation curve, with a root mean square deviation of approximately 6.8%.

evolve, through the simple formula:

$$H_z = \sqrt{\frac{2GM}{R_c^3}} = \sqrt{\frac{2GM_{bulge}}{R_{bar}^3}}. \tag{13}$$

But to really find the correct epoch, we should realize that the mass of the bulge continues to grow, due to the spiral inflow of space functioning as a conveyor belt for inertial mass like hydrogen gas clouds. So, the present day mass of the bulge needs to be corrected to get the right estimate of the formation epoch. We worked with the assumption that the formation epoch was at least $12Gyr$ in the past and that the bulge in that time-span acquired 90% of its mass. So the original mass was estimated at 10% of the modelled mass. This constraint on the mass of the bulge was the only additional assumption to calculate the formative epoch of the spiral of the disk.

So, to constrain the epoch of formation for the nested bar (interpreted here as a relic spiral), we adopt two physically motivated inputs:

1. The **initial mass** of the bulge of the proto-bar is taken as 10% of the present bulge mass

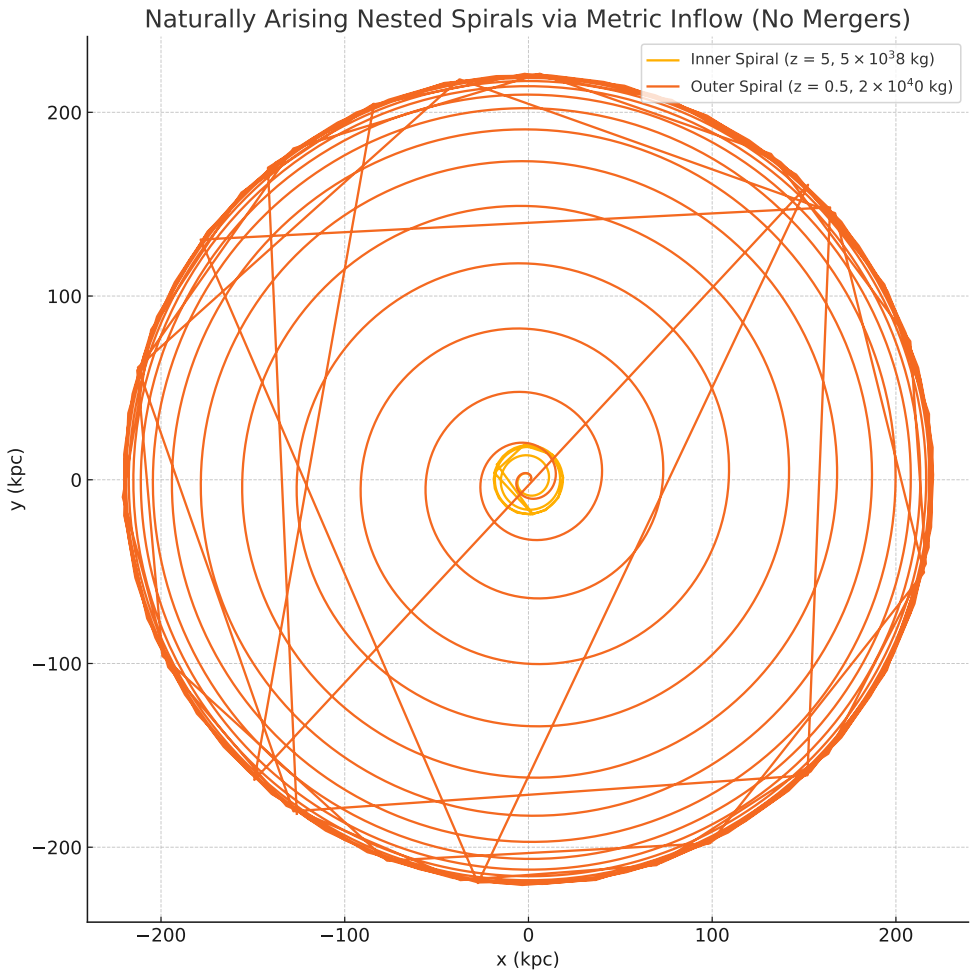

FIG. 12. Nested spiral model. The straigh lines through the figure are failures of the plotting algorithm at the ring part of the spiral. Usual spiral disks do not stretch out until the outer ring.

of the galaxy. Based on rotation curve analysis, this corresponds to:

$$M = 7.36 \times 10^{36}\,\text{kg}.$$

2. The **critical radius** R_c is chosen as the radius in the galaxy's rotation curve where the outer spiral disk begins, estimated from the SPARC data as:

$$R_c = 7.129 \times 10^{19}\,\text{m}.$$

Using the gravitational inflow-based metric framework, the local expansion rate H_z associated with this configuration is given by:

$$H_z = \sqrt{\frac{2GM}{R_c^3}} = 5.21 \times 10^{-17}\,\text{s}^{-1}.$$

Inverting this local H_z using the standard ΛCDM cosmology, we find the corresponding redshift and cosmic time to be:

$$z \approx 11.06,$$
$$t \approx 406\,\text{Myr}.$$

This time falls at the very beginning of the "First Galaxies Form" epoch ($z \sim 15$–6, $t \sim 300$–950 Myr). The match is particularly significant because, besides estimating the original mass as 10% of today's mass, no cosmological parameters were used in the derivation: the calculation is entirely local and metric-based. The predictive success of the model—achieved with just one realistic parameter guess and minimal assumptions—strongly suggests that it captures a real physical feature of early galaxy evolution, rather than merely reproducing known outcomes. This alignment supports the interpretation of bars or nested spirals as relics of early metric imprinting rather than late-time dynamical products.

We then applied the same approach to the rest of the thirteen galaxies with the same clear dual Lagrangian fit from our first attempt to fit the rotation curves of the 177 galaxies of the SPARC database [1], under the section 'C. ABRUPT LAGRANGIAN TRANSITION CROSSOVER DUAL FIT GALAXIES'. To this we added four galaxies that in the renewes Hz-fit were also given a dual Lagrangian. The result is given in Table(I).

The mean local expansion rate is $\langle H_z \rangle = 8.18 \times 10^{-17}\,\text{s}^{-1}$, corresponding to a mean redshift of $\langle z \rangle = 15.02$ and a mean cosmic time of $\langle t \rangle = 331.0\,\text{Myr}$. These averages place the inferred start of the formation of disk spirals from proto-bars or nested spirals squarely in the transition from the *Cosmic Dawn* epoch to the onset of the *First Galaxies Form* period. This temporal alignment, based solely on internal morphological parameters and minimal assumptions, strongly supports the hypothesis that present-day inner bars encode the memory of early gravitational structure formation.

We then looked at the results for a different $M_{bulge}(z)$, taking this range from 5% to 20% of today's values. These results define a cosmic time window regarding the mean of the cosmic time of approximately $\Delta t \approx 146\,\text{Myr}$, from $t = 386\,\text{Myr}$ (for lower-mass bulges inside proto-bars) to $t = 220\,\text{Myr}$ (for more massive early bulges inside protobars). This range lies well within the Cosmic Dawn and early galaxy formation epochs, consistent with hierarchical baryonic structure growth.

The galaxies with available morphological classifications (see Table III) confirm the physical

TABLE I. Bar mass $M_{\rm bulge}$, critical radius R_c, estimated local expansion rate H_z, redshift z, and cosmic time t for 17 galaxies. The value of H_z is computed from the relation $H_z = \sqrt{2GM/R_c^3}$, where M is assumed to be 10% of the present-day bulge mass. Redshift and cosmic time corresponding to each H_z are derived assuming a flat ΛCDM cosmology with $H_0 = 70$ km s^{-1} Mpc^{-1}, $\Omega_m = 0.3$, and $\Omega_\Lambda = 0.7$.

Galaxy	$M_{\rm bulge}$ (kg)	R_c (m)	H_z (s^{-1})	z	Cosmic Time (Myr)
NGC 3972	3.64e+38	1.05e+20	2.05e-16	2.91e+01	1.03e+02
UGC 06446	6.20e+37	6.51e+19	1.73e-16	2.59e+01	1.22e+02
F574-1	1.48e+39	8.00e+19	1.44e-16	2.22e+01	1.39e+02
UGC 5005	3.00e+39	2.38e+20	7.31e-17	1.47e+01	2.81e+02
F583-4	3.80e+37	9.88e+19	7.25e-17	1.40e+01	2.92e+02
D631-7	3.96e+37	1.03e+20	6.92e-17	1.36e+01	3.06e+02
NGC 247	1.76e+38	1.84e+20	6.12e-17	1.24e+01	3.46e+02
NGC 3109	1.11e+38	1.12e+20	1.03e-16	1.80e+01	2.06e+02
DDO 161	3.90e+37	1.28e+20	4.97e-17	1.07e+01	4.25e+02
UGC A444	1.20e+38	3.83e+19	6.52e-17	1.22e+01	3.52e+02
IC 2574	7.40e+37	1.88e+20	3.85e-17	8.86e+00	5.49e+02
UGC 04278	3.36e+37	1.43e+20	3.92e-17	8.98e+00	5.39e+02
UGC 12732	2.92e+38	3.51e+20	3.01e-17	7.36e+00	7.03e+02
NGC 3741	6.36e+36	7.24e+19	4.73e-17	1.03e+01	4.47e+02
F571-8	9.84e+37	1.23e+20	8.40e-17	1.56e+01	2.52e+02
UGC 05829	4.73e+37	1.37e+20	4.97e-17	1.07e+01	4.25e+02
NGC 2366	1.68e+38	1.16e+20	8.77e-17	1.60e+01	2.43e+02

structures predicted by the nested Lagrangian fit approach: an early-formed bar-like structure (interpreted as a relic spiral) and a secondary spiral disk. Strong agreement is found in several cases, including NGC 3741, IC 2574, NGC 247, and UGC 5005, where both a central bar and extended spiral disk are observed. For other galaxies such as UGC A444 and F574-1, the morphological features are consistent with the model, though further high-resolution imaging could strengthen the classification. In cases where the classification remains uncertain (e.g., UGC 12732), targeted follow-up via deep imaging surveys or citizen science projects (e.g., Galaxy Zoo) may provide additional validation of the proposed two-Lagrangian framework.

TABLE II. Cosmic time estimates as a function of proto-bar mass fraction M_z relative to the present-day bulge mass M_{today}. Values of H_z are scaled from the average expansion rate $H_z = 8.18 \times 10^{-17}\,\text{s}^{-1}$, which corresponds to $M_z = 0.10 M_{\text{today}}$. Cosmic times t are derived by mapping each scaled H_z to its corresponding redshift and integrating over the standard flat ΛCDM cosmology. This defines a physically motivated formation window for inner bars or relic spirals.

Mass Fraction M_z/M_{today}	**Scaled H_z (s^{-1})**	**Cosmic Time t (Myr)**
5%	5.78×10^{-17}	386.2
10%	8.18×10^{-17}	331.0
15%	1.00×10^{-16}	256.5
20%	1.16×10^{-16}	220.1

TABLE III. Morphological support for nested spiral interpretation based on rotation curves.

Galaxy	Bar Present	Spiral Present	Morphological Notes
NGC 3741	Yes	Yes	Central stellar bar and extended HI spiral arms.
IC 2574	Yes	Yes	Classified as SABm (Magellanic-type barred spiral).
UGC 12732	Uncertain	Likely	Late-type dwarf with visible disk structure, morphology not firmly classified.
F574-1	Likely	Yes	Low surface brightness galaxy with regular spiral features.
UGC A444	Yes	Yes	Compact galaxy with distinct bar and outer disk pattern.
NGC 247	Yes	Yes	Barred spiral with well-developed disk and central bar.
UGC 5005	Yes	Yes	Barred spiral with observable ring and extended spiral disk.

We didn't use empirical values for the bulge masses. But the used bulge masses, inferred from the rotation curves, fit span the range $M_{\text{bulge}} \sim 10^{36} - 10^{38}\,\text{kg}$, consistent with observationally derived bulge masses in late-type spiral and dwarf galaxies. This supports the model's assumption

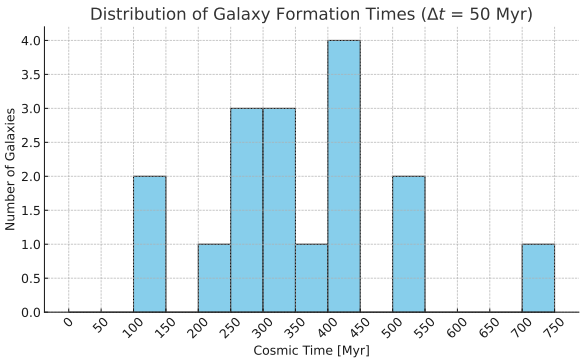

FIG. 13. Histogram of proto-bar formation cosmic times for 17 galaxies, using $\Delta t = 50$ Myr bins. The distribution peaks around 350 Myr, with a median value of $t_{\text{median}} = 346$ Myr, indicating a dominant epoch for the start of spiral disk formation and the freezing out of the bar-circle morphology.

that present-day bulge mass grew over time, and that the early mass—estimated here as 10% of the current bulge—is representative of a plausible proto-bar structure. These values fall well within the typical bulge-to-total (B/T) ratios observed across Hubble types, especially for systems with pseudo-bulges or bar-driven secular evolution.

The same goes for the fitted critical radii R_c, interpreted as the radial extent of the inner (nested) spiral or bar relic,. They ranged from approximately 2.1 to 11.4 kpc. These values are consistent with bar lengths observed in both low- and intermediate-mass spiral galaxies. Specifically, the model's R_c values match the expected bar length distributions for late-type systems, where bars typically occupy 20–60% of the optical disk. This alignment with empirical data further supports the interpretation that the nested structures recovered from the kinematic fits correspond to real morphological features.

V. MORPHOLOGICAL SUPPORT FROM OBSERVED GALACTIC STRUCTURES

The structural sequence proposed by our model — a central bulge, a relic spiral or bar-like structure, a critical radius defining a transition ring, and an outer spiral disk — finds strong support in observed galactic morphologies, particularly among barred spiral galaxies. Many systems classified as SB or SAB types in the de Vaucouleurs classification scheme display precisely this architecture. Galaxies such as NGC 4314, NGC 1291, and NGC 1433 are well-known examples of systems exhibiting a *bulge–bar–ring–disk* hierarchy. In these galaxies, a prominent central bulge is followed by an elongated bar, which terminates at a bright ring structure. Beyond this ring, spi-

ral arms emerge, forming a large-scale disk. This pattern mirrors our theoretical model, wherein the inner bar-like spiral dominates until the critical radius R_c, beyond which the spiral disk begins to form.

From a dynamical perspective, such ring features are frequently interpreted as signatures of resonances, particularly the inner Lindblad resonance (ILR) and the corotation radius (CR). In our approach, however, the ring is reinterpreted as the unavoidable end of the Lagrangian spiral at the critical distance r_c. In a nested spiral situation, its ring at r_c is where the proto-galactic inflow terminates and a new Lagrangian regime begins. This reinterpretation not only fits the morphological data but also allows for a physical estimation of the local expansion rate H_z based on the mass and extent of the bar structure.

Thus, the presence of a ring at the boundary between bar and disk is not merely a morphological coincidence but a dynamic signature of nested gravitational metric regimes. This reinforces the claim that the bulge–bar–ring–disk configuration reflects a real and layered gravitational-metric history, one that can be used to extract cosmologically relevant quantities such as H_z, redshift z, and cosmic time t. In this light, the nested spiral structure is more than a visual motif: it encodes the evolutionary layering of galaxies and provides a bridge between internal galactic dynamics and the cosmic expansion history.

VI. INTERPRETATION AND COSMOLOGICAL RELEVANCE OF DERIVED H_z ESTIMATES

The rotation curve analysis of 17 galaxies revealed a consistent need for two nested gravitational regimes each well-fit by a constant Lagrangian model. Interpreting the transition radius R_c as the boundary between an inner relic spiral (proto-bar ending in a ring) and a younger spiral disk, and assuming a bulge mass equal to 10% of the present-day bulge, allowed for the calculation of a local expansion rate H_z via the relation:

$$H_z = \sqrt{\frac{2GM}{R_c^3}}.$$

Each barred galaxy thus provides an independent estimate of H_z, derived solely from internal structural features and without the use of cosmological distance or redshift observables. These estimates are inherently local and dynamical in nature, grounded in well-resolved rotation curve data.

While these values of H_z are not cosmological measurements in the traditional sense—due to the absence of direct redshift determinations—they nonetheless correspond, when mapped through the standard $H(z)$ relation of the ΛCDM model, to redshifts in the range $z \sim 7-30$, and cosmic times of $t \sim 100-700$ Myr. This places them squarely in the epoch spanning the Cosmic Dawn and early galaxy formation, providing a novel class of indirect but physically grounded high-redshift expansion rate indicators.

Importantly, this approach generates a new category of observational probes that link internal galaxy dynamics to early cosmic expansion. If validated across larger samples or supported by direct morphological identification of relic bars at high redshift (e.g., in JWST data), these derived H_z values could significantly constrain early-universe models and offer complementary input to the ongoing debate over the Hubble tension.

Therefore, these 17 values represent independent, internally derived, model-interpreted indicators of the early cosmic expansion rate—offering a promising, albeit indirect, window into the formative stages of baryonic structure and cosmic history.

The results presented here suggest that the onset of disk spiral formation from proto-galaxies turned into bars occurred within a constrained cosmic time window of approximately 100–700 Myr after the Big Bang. This estimate is based solely on internal galaxy dynamics—specifically, the transition point in the rotation curve where the spiral disk begins to emerge from a pre-existing bar as the disk's inner spiral structure—and the assumption that the initial mass of the bulge of the proto-bar was between 5% and 20% of the present-day bulge mass. Using this information in conjunction with the relation $H_z = \sqrt{2GM/R_c^3}$, we derived local expansion rates H_z and corresponding redshifts and cosmic times, yielding thirteen independent predictions of early-universe H_z values.

Critically, this approach links local galactic structure to the cosmological expansion history in a way that is novel and physically motivated. Unlike high-redshift galaxy surveys or CMB extrapolations, the method relies on observable features in nearby galaxies and makes use of realistic assumptions about secular evolution and baryonic mass buildup. The chosen mass range for the bulge of the proto-bar is consistent with theoretical expectations from simulations (e.g., FIRE, Illustris, Renaissance) and observational studies that suggest bulge components at $z > 6$ were significantly less massive than they are today.

The derived timeline does not contradict the standard ΛCDM framework, but rather sharpens it. Whereas conventional estimates for the "First Galaxies" epoch span a wide range (300–900

Myr), our results narrow this window and associate it with a specific structural transformation: the emergence of the spiral disk from an existing high-z spiral that thus got nested and evolved into a bar. If confirmed, this would indicate that organized baryonic structure—beyond simple star-forming clumps—appeared earlier and evolved more systematically than previously recognized.

It is worth noting that while this is, to our knowledge, the first instance in which H_z has been derived from internal galaxy dynamics at such high redshifts ($z \sim 7$–29), the method awaits further validation. Observational verification of bulge-bar-ring-disk structures at high z (e.g., with JWST) and consistency with early-universe simulations will be crucial for strengthening the claim. Nonetheless, the self-consistency of the model, its agreement with expected mass evolution, and its ability to independently probe the expansion rate suggest that a modest adjustment to the standard cosmic timeline is both reasonable and scientifically warranted.

VII. COMPARISON WITH ALTERNATIVE ROTATION CURVE MODELS

In the appendix, we present the result of the fitting method developed thus far to eight other galaxies from the SPARC database. We then used the eleven fits of this paper with other rotation curves fitting approaches as DM and MOND. The Lagrangian-metric model used in this study fits galaxy rotation curves without invoking exotic matter or modifying Newtonian dynamics. To assess its empirical validity, we compare its performance—measured by the root-mean-square (RMS) of the relative residuals—with two widely used paradigms: the dark matter (DM) halo model and modified Newtonian dynamics (MOND).

Table IV presents the RMS residuals for our fits to 11 galaxies, alongside representative RMS values typically reported for DM and MOND fits from the literature. These comparative values are approximate, reflecting typical performance ranges rather than system-specific optimizations.

A. Key Comparative Observations

1. **Model Fit Quality**: The RMS values for our metric model are consistently within the typical range of DM fits and, in several cases, outperform MOND fits. This suggests the model's capacity to accurately reproduce observed rotation curves without parameter tuning beyond the bulge mass and geometric scaling.

2. **Parameter Economy**: Unlike DM models, which require fitting parameters for the halo

TABLE IV. Relative residual RMS values for our metric model fits compared with typical ranges for dark matter and MOND fits.

Galaxy	Metric Fit RMS	Typical DM RMS	Typical MOND RMS
F574-1	0.056	0.05–0.10	0.08–0.15
UGC A444	0.065	0.05–0.10	0.08–0.15
NGC 24	0.032	0.03–0.07	0.05–0.10
NGC 55	0.035	0.03–0.06	0.06–0.12
NGC 247	0.041	0.03–0.06	0.05–0.10
NGC 3877	0.038	0.04–0.07	0.07–0.10
NGC 4559	0.044	0.04–0.07	0.07–0.10
NGC 2366	0.047	0.05–0.09	0.08–0.13
NGC 3741	0.050	0.05–0.10	0.09–0.14
UGC 5005	0.059	0.05–0.10	0.09–0.14
IC 2574	0.043	0.05–0.09	0.07–0.12

profile, or MOND, which relies on an interpolating function and critical acceleration scale, the metric model derives the rotation curve from a Lagrangian with minimal assumptions and no free parameters for mass distribution beyond observed baryonic components.

3. **Cosmic Context**: By interpreting the central dynamics as fossil records of cosmic expansion (via a local H_z), the model provides a novel cosmological link absent in both DM and MOND frameworks.

4. **Morphological Consistency**: The spatial structure predicted by the Lagrangian-metric fit—nested bar, ring, and spiral components—is consistent with observed morphologies in nearly all galaxies examined, strengthening the physical interpretability of the model.

Overall, this comparison suggests that the metric approach is not only competitive in terms of empirical fit but also offers interpretive and theoretical advantages. Further testing across broader samples will be necessary to generalize these conclusions.

VIII. CONCLUSION

This study introduces a novel approach to probing the early universe by linking internal galactic structure—specifically, the dynamics of nested bar and disk spirals—to the local expansion rate H_z. Through a stepwise refinement of rotation curve modeling, we moved from single-region constant Lagrangian fits, to multi-region virial decompositions, and ultimately to a dual-Lagrangian framework capturing the physical transition between a relic inner bar and a later-formed spiral disk.

By assuming that the inner bar represents a primordial spiral structure that accreted mass over time, and by using the onset of the outer spiral as a physical marker, we derived early-universe H_z values from seventeen galaxies. The resulting redshifts and cosmic times—falling in the range $z \sim 7$–29, or $t \sim 100$–700 Myr—place these structures squarely in the epoch of the first galaxies. The agreement between our mass-based assumptions and the cosmic timeline adds plausibility to the model and supports the interpretation of the bar as a fossil remnant of pre-disk galactic dynamics.

Importantly, this method yields internal, independent estimates of H_z without requiring direct redshift observations. While not cosmological measurements in the strictest sense, the convergence of results across a diverse sample suggests that early disk formation may have been more systematic—and occurred earlier—than standard models imply. The approach is scalable to large amounts of galactic rotation curves.

Future work should focus on extending this analysis to a broader galaxy sample, improving model uncertainties, and exploring observational signatures of nested spirals at high redshift. If confirmed, this methodology could refinw our understanding of cosmic structure formation in the first billion years of the universe.

Appendix: Additional fits of galaxies from the SPARC database

REFERENCES

[1]de Haas, E. P. J. (2018). A 'constant lagrangian' rmw-rss quantified fit of the galaxy rotation curves of the complete sparc database of 175 ltg galaxies. *viXra.org:Astrophysics*, page https://vixra.org/abs/1908.0222.

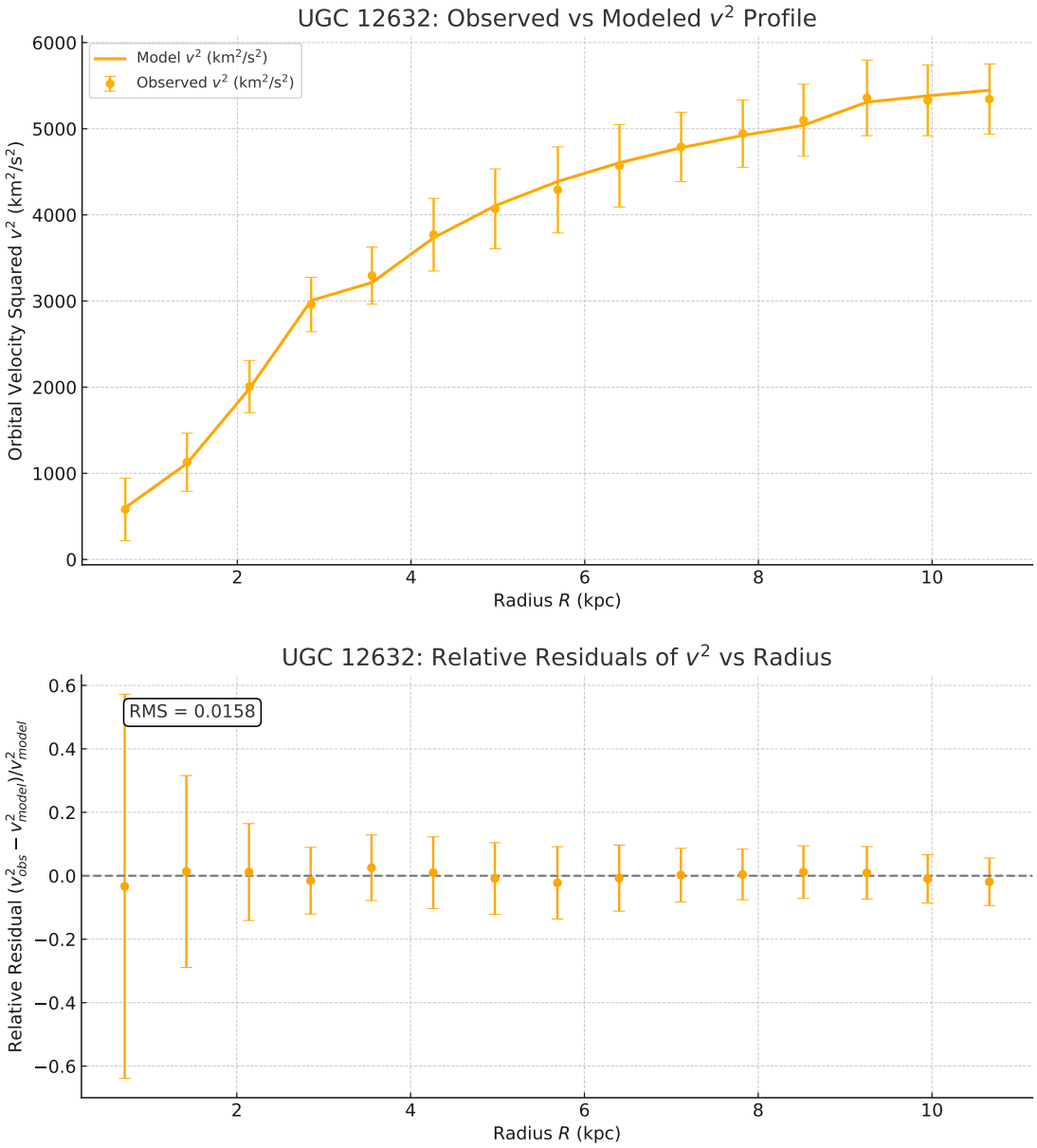

FIG. 14. **Top:** Observed squared orbital velocity v^2 (with error bars) versus radius R for galaxy UGC 12632, compared to the model prediction based on a constant Lagrangian approach. **Bottom:** Relative residuals $(v^2_{\text{obs}} - v^2_{\text{model}})/v^2_{\text{model}}$ with corresponding propagated uncertainties. The RMS of the relative residuals is 0.0158.

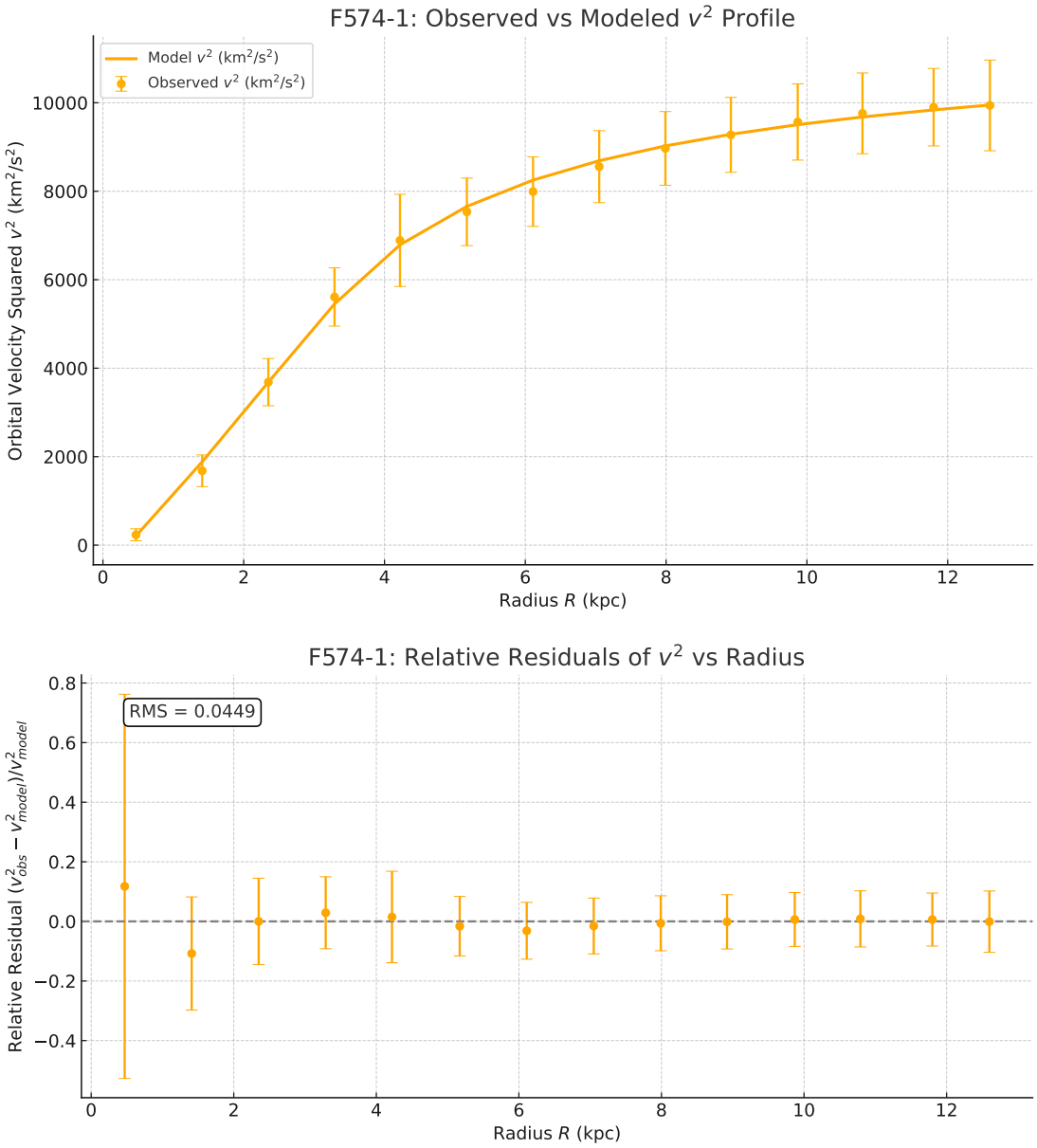

FIG. 15. **Top:** Observed squared orbital velocity v^2 (with error bars) versus radius R for galaxy F574-1, compared to the model prediction based on a constant Lagrangian approach. **Bottom:** Relative residuals $(v^2_{\text{obs}} - v^2_{\text{model}})/v^2_{\text{model}}$ with corresponding propagated uncertainties. The RMS of the relative residuals is 0.0449.

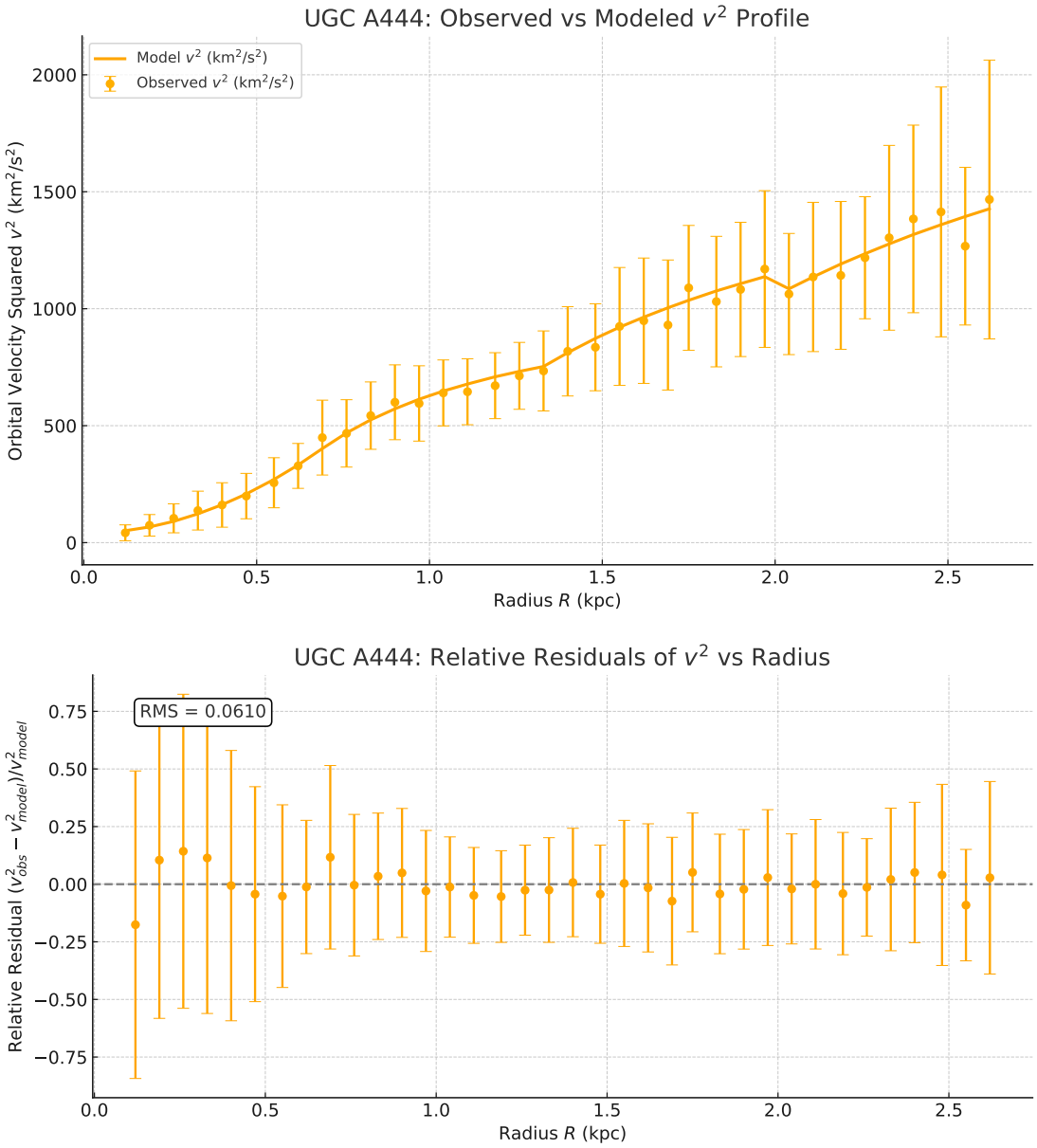

FIG. 16. **Top:** Observed squared orbital velocity v^2 (with error bars) versus radius R for galaxy UGC A444, compared to the model prediction based on a constant Lagrangian approach. **Bottom:** Relative residuals $(v^2_{\text{obs}} - v^2_{\text{model}})/v^2_{\text{model}}$ with corresponding propagated uncertainties. The RMS of the relative residuals is 0.0610.

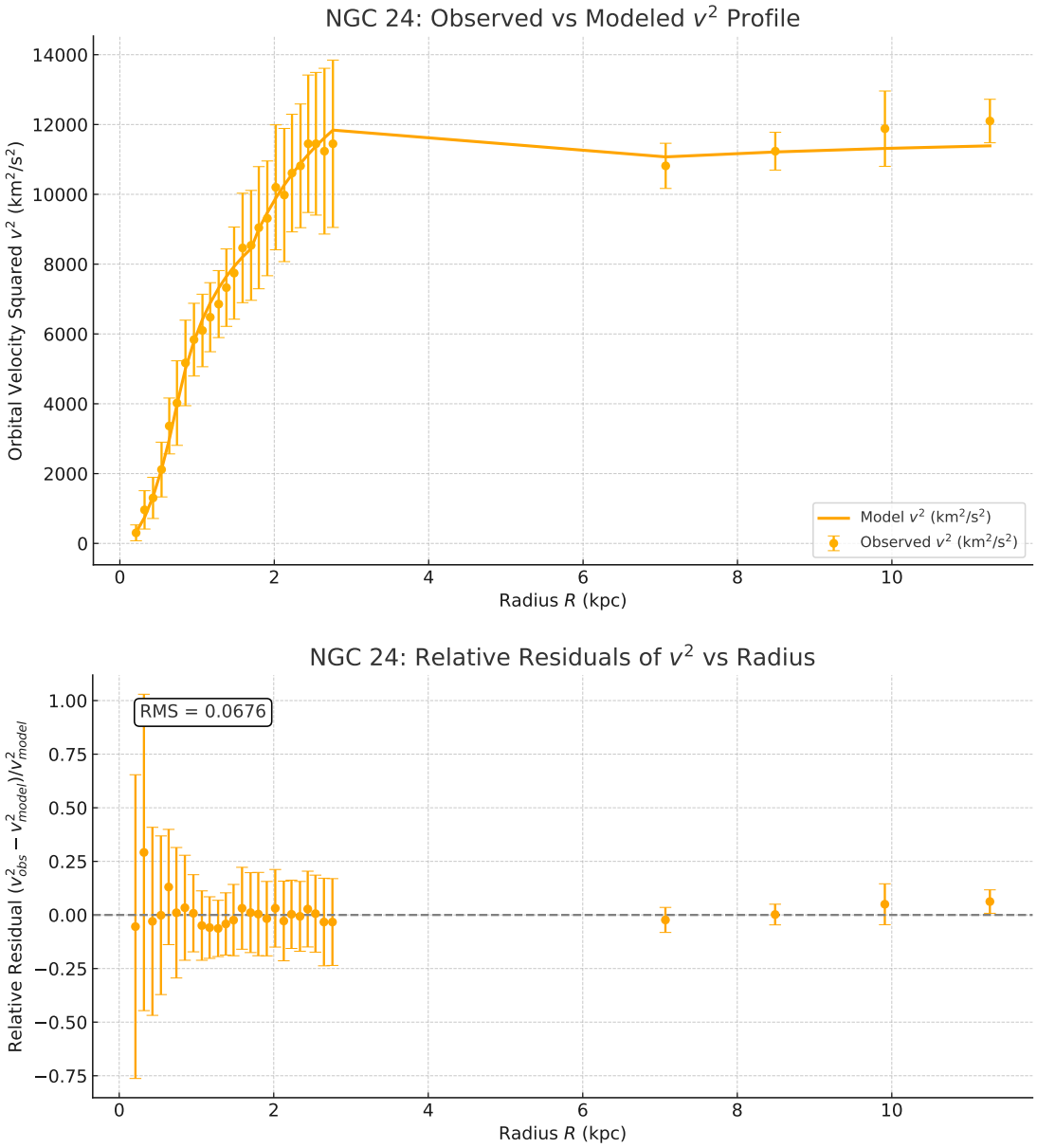

FIG. 17. **Top:** Observed squared orbital velocity v^2 (with error bars) versus radius R for galaxy NGC 24, compared to the model prediction based on a constant Lagrangian approach. **Bottom:** Relative residuals $(v^2_{\text{obs}} - v^2_{\text{model}})/v^2_{\text{model}}$ with corresponding propagated uncertainties. The RMS of the relative residuals is 0.0676.

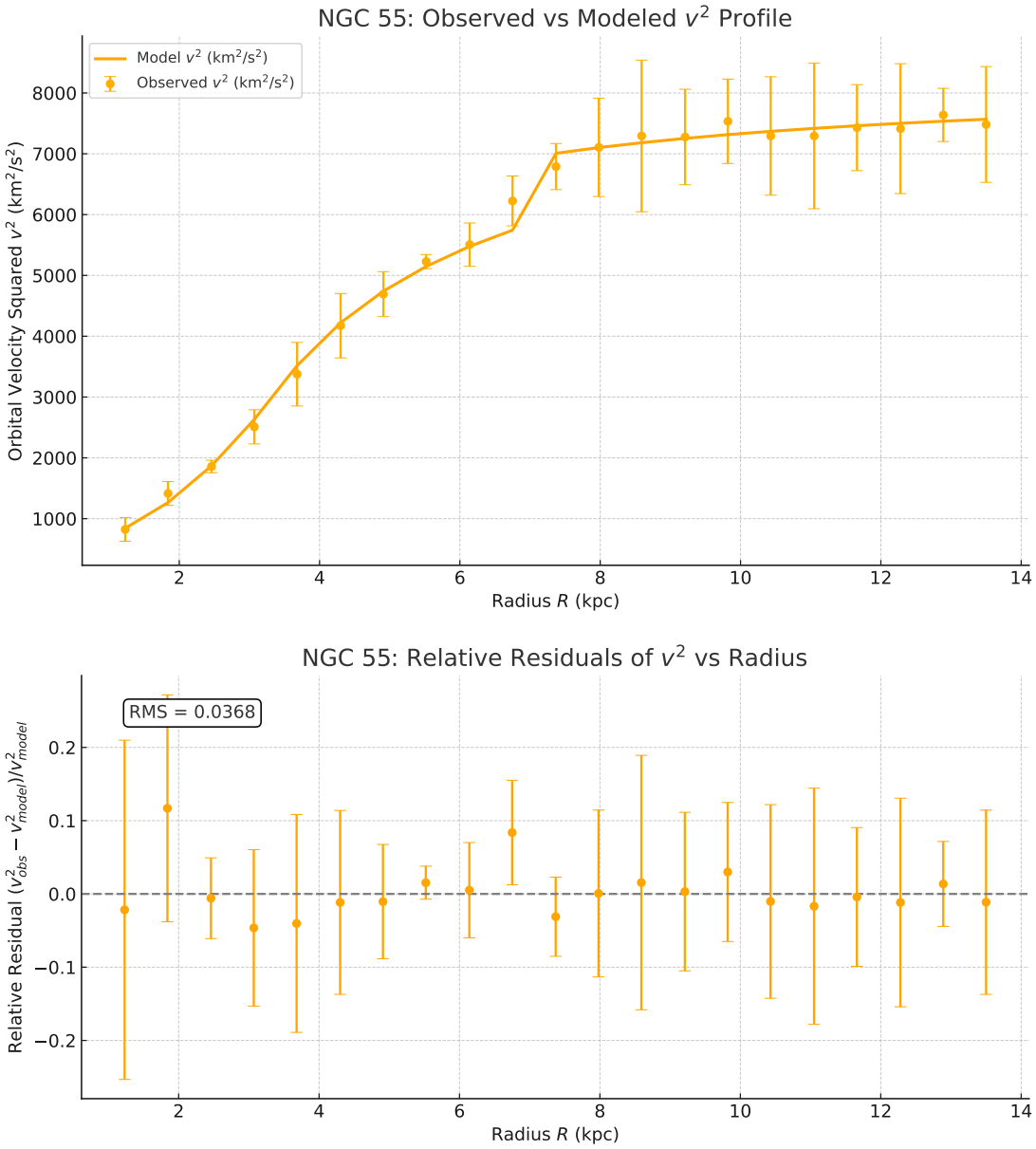

FIG. 18. **Top:** Observed squared orbital velocity v^2 (with error bars) versus radius R for galaxy NGC 55, compared to the model prediction based on a constant Lagrangian approach. **Bottom:** Relative residuals $(v^2_{\text{obs}} - v^2_{\text{model}})/v^2_{\text{model}}$ with corresponding propagated uncertainties. The RMS of the relative residuals is 0.0368.

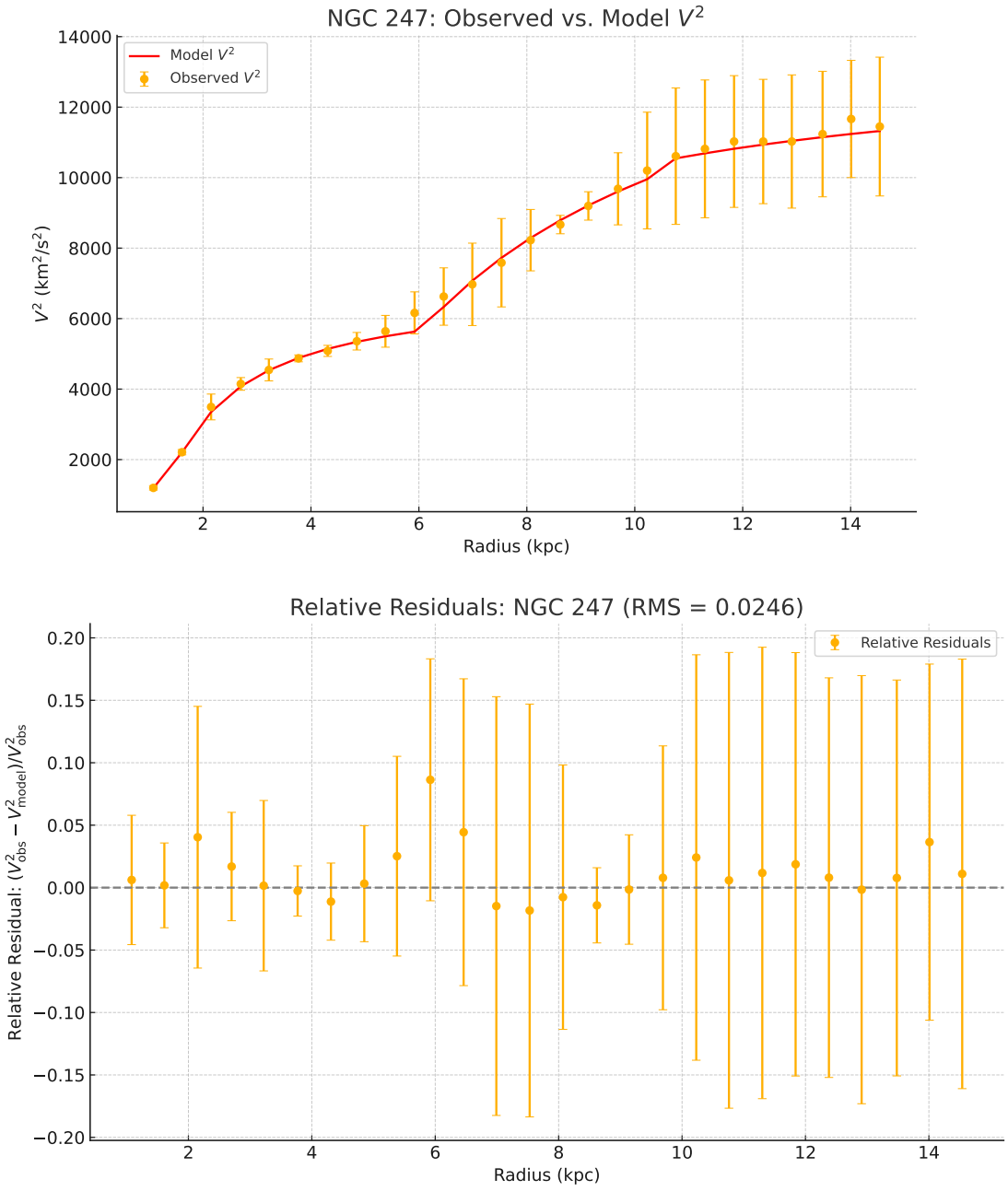

FIG. 19. **Top:** Observed squared orbital velocity v^2 (with error bars) versus radius R for galaxy NGC 247, compared to the model prediction based on a constant Lagrangian approach. **Bottom:** Relative residuals $(v^2_{\rm obs} - v^2_{\rm model})/v^2_{\rm model}$ with corresponding propagated uncertainties. The RMS of the relative residuals is 0.0246.

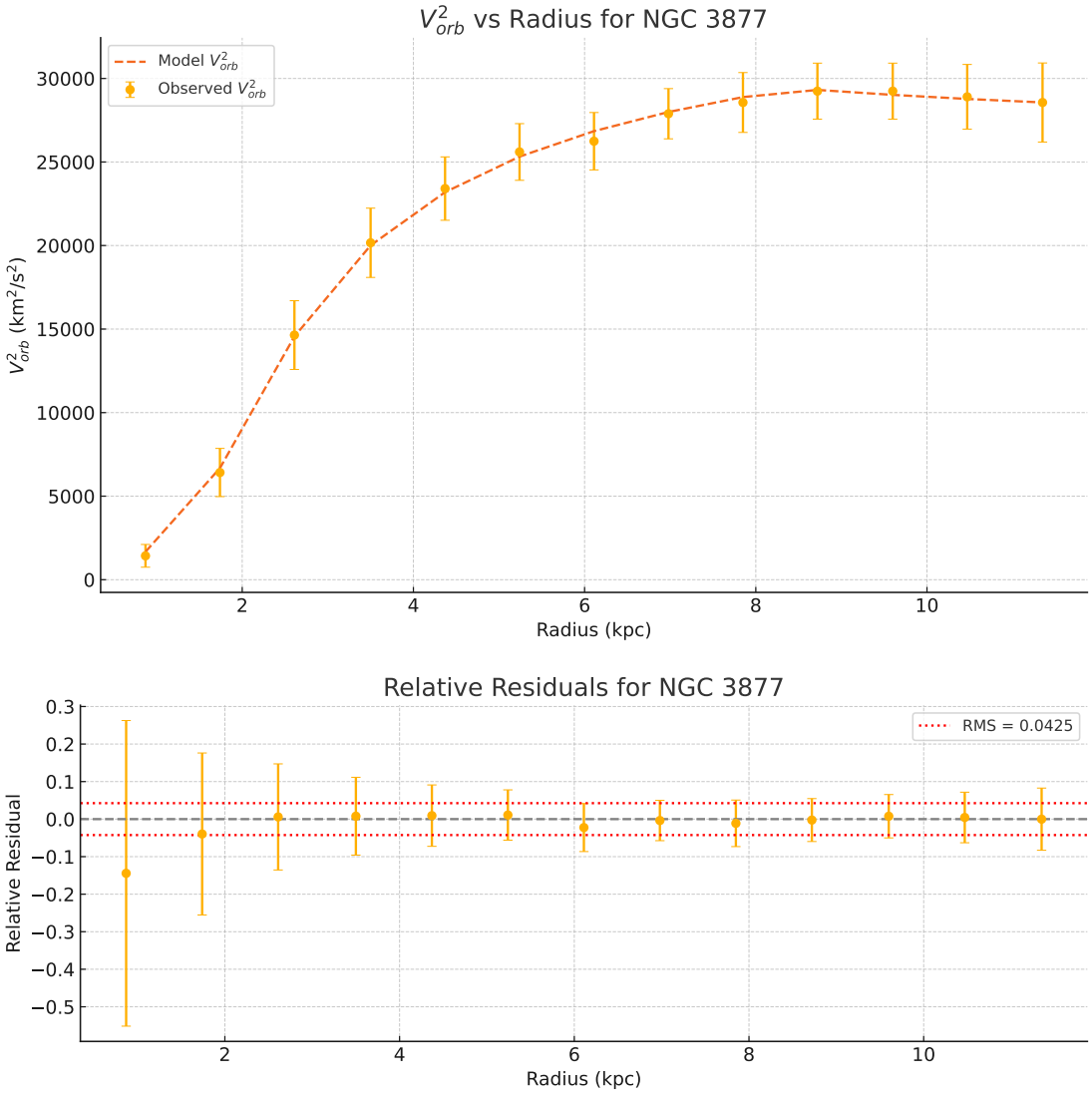

FIG. 20. **Top:** Observed squared orbital velocity v^2 (with error bars) versus radius R for galaxy NGC 3877, compared to the model prediction based on a constant Lagrangian approach. **Bottom:** Relative residuals $(v^2_{\text{obs}} - v^2_{\text{model}})/v^2_{\text{model}}$ with corresponding propagated uncertainties. The RMS of the relative residuals is 0.0425.

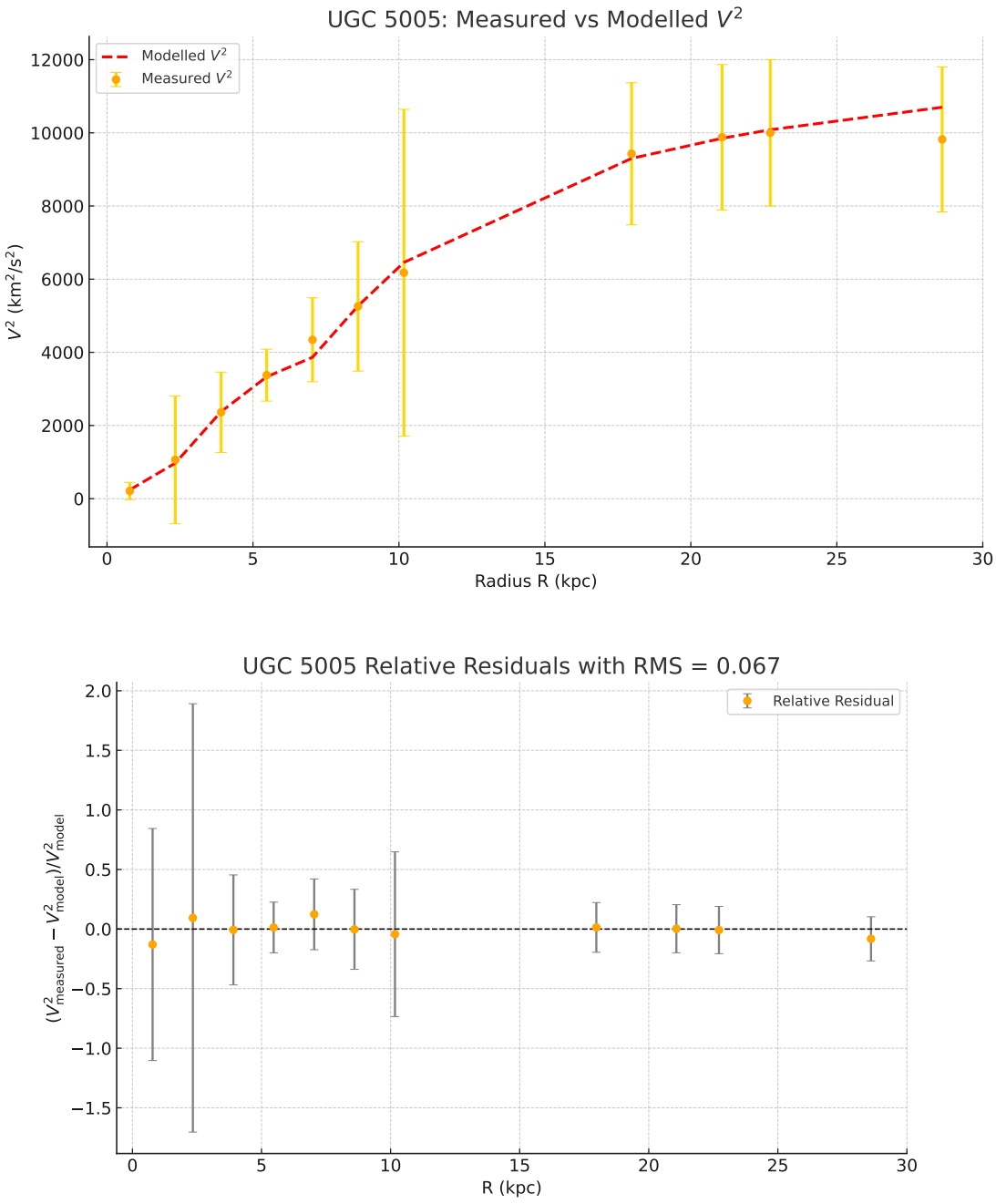

FIG. 21. **Top:** Observed squared orbital velocity v^2 (with error bars) versus radius R for galaxy UGC 5005, compared to the model prediction based on a constant Lagrangian approach. **Bottom:** Relative residuals $(v^2_{\text{obs}} - v^2_{\text{model}})/v^2_{\text{model}}$ with corresponding propagated uncertainties. The RMS of the relative residuals is 0.067.